Adsorption (2014) 20:21–35
DOI 10.1007/s10450-013-9545-0

Linking pore diffusivity with macropore structure of zeolite adsorbents. Part II: simulation of pore diffusion and mercury intrusion in stochastically reconstructed zeolite adsorbents

E. S. Kikkinides · M. G. Politis

Received: 14 December 2012 / Accepted: 28 March 2013 / Published online: 7 April 2013

Abstract In the present study we complete the evaluation of three dimensional digitized reconstructions of a binderless zeolite adsorbent with improved mass transfer rates, by performing simulations of pore diffusion and Hg-intrusion porosimetry in these structures. It is seen that an excellent agreement with the experimental diffusivity is achieved (relative error of 1.2 %) for a pore structure that matches, besides low order correlations, chord length distribution functions that account for higher order correlations. Furthermore, simulations on a variety of reconstructed samples indicate that matching chord length distribution functions is a necessary (though probably not sufficient) condition for accurate structural representation. The average tortuosity factor is 2.68 and is nearly constant over a broad spectrum of pressures, when properly normalized. Hg-intrusion porosimetry simulations, performed with a pure morphology method, show a good agreement with the experimental curve for normalized cumulative intrusion volumes in the range of 50–88 %, but cannot make a distinction between structures with differences in higher order correlations. It is believed that SEM micrographs, properly obtained to represent realistic 2D sections of the material, contain sufficient structural information that can distinguish among pore structures with different mass transfer rates, when combined with stochastic reconstruction methods. Evidently, the direct link between these structural parameters and pore diffusivity will provide the necessary route to improve the mass transfer rate of porous adsorbents.

Keywords Stochastic reconstruction · Pore diffusion simulation · Random walk methods · Mercury porosimetry · Drainage simulation · Zeolite adsorbents

E. S. Kikkinides (✉) · M. G. Politis
Department of Mechanical Engineering, University of Western Macedonia, Bakola & Sialvera Str., 50100 Kozani, Greece
e-mail: kikki@cperi.certh.gr

E. S. Kikkinides · M. G. Politis
Chemical Process and Energy Resources Institute (CPERI), Centre for Research and Technology Hellas (CERTH), P.O. Box 60361, 57001 Thessaloniki, Greece

1 Introduction

In part I of this series (Kikkinides and Politis 2013) we have reported on the three-dimensional representation of the structure of a binderless zeolite adsorbent that was previously developed and meets the targets of N_2 pore diffusivity, $D_{p,N_2} \geq 3.5 \times 10^{-6} \mathrm{m}^2/\mathrm{s}$, at a pressure of 1.5 bar and temperature of 300 K (Ackley and Leavitt 2002; Chao and Pontonio 2002; Ackley et al. 2003). More specifically, we have employed the simulated annealing (SA) technique, starting either from a purely random structure (standard SA method) or from a random sphere pack (hybrid method), and have generated three-dimensional porous structures that match the basic low order correlations (porosity and two-point correlation function), measured on two-dimensional SEM images of the actual materials. Furthermore, we have evaluated the porous structures produced by each reconstruction method (standard SA or hybrid) by measuring, besides porosity and two-point correlation function, chord length distribution functions that account for higher order correlations in the porous matrix. It is found that the hybrid method with an initial temperature, $T = 1 \times 10^{-10}$, produces porous structures that match, besides porosity and two-point correlation function, pore and mass chord length distribution functions. The standard SA method, on the

other hand, while matching porosity and two point correlation, it fails to match pore and mass chord length distribution functions. We have attributed this difference in pore structure to the fact that the hybrid method preserves parts of the original sphere pack configuration found in the initial zeolite powder used in the actual fabrication process of the adsorbent.

In part II, we further evaluate each developed structure by simulating N_2 diffusion using a step by step Monte Carlo random walk process and Hg-intrusion porosimetry employing a pure morphology method. The resulting N_2 pore diffusivities and Hg-intrusion curves for each structure are compared with each other and with experiments, in an attempt to show how pore diffusion and Hg-intrusion are affected by structural differences and which reconstruction method is more suitable in the case of the zeolite adsorbent examined in the present study. Evidently, the ultimate goal of this series of publications is to identify the main structural characteristics that control the mass transfer rate in the zeolite adsorbent. It is expected that improvement of these selected key structural parameters will enhance mass transfer rate in the adsorbent and hence process performance characteristics in a PSA/VSA operation.

2 Theoretical section

2.1 Gas diffusion in porous media

Gas diffusion in porous media, usually called pore diffusion, is characterized by the resistance that a gas encounters as it diffuses through the pore space of a porous material (Karger and Ruthven 1992). This resistance is a function of the molecular properties of the gas, its interaction with the internal surface and the internal architecture of the porous matrix. Diffusion of small gas molecules in the macropore space of a zeolite adsorbent depends primarily on the latter (Karger et al. 1981; Karger and Ruthven 1992; Ruthven and Xu 1993; Papadopoulos et al. 2007). Hence, in this case, the complex pore structure results in lowering the diffusion coefficient in the unconstrained free space by a simple geometric factor that is often called tortuosity (Satterfield and Sherwood 1963). Therefore, when studying pore diffusion, it is important first to determine accurately diffusion coefficients in the free space before we refer to the case of diffusion in the porous matrix of the material.

2.2 Estimation of self-diffusion coefficients

The simplest derivation of an expression for self-diffusivity, D, of an ideal gas uses Maxwell's expression for the mean free path, λ, together with a simplistic approximation for the mean molecular velocity. Simple momentum exchange principles result in the following classic expression from the Kinetic Theory of Gases (Jeans 1925; Kennard 1938):

$$D = \frac{1}{3}\lambda\bar{u} \tag{1}$$

where $\bar{u} = \left(\frac{8R_gT_g}{\pi M}\right)^{1/2}$ is the mean thermal speed of the gas with molecular weight M, T_g is the gas temperature and R_g the universal gas constant. The mean free path, λ, for the case of self diffusion of a gas with number density n, and molecular collision diameter, σ, is often described as Maxwell's mean free path and it is given by the well known expression from the Kinetic theory of gases (Jeans 1925; Kennard 1938):

$$\lambda = \frac{1}{\pi n\sigma^2\sqrt{2}} = \frac{kT_g}{s(P\times 10^5)\sqrt{2}} \tag{2}$$

where k = Boltzmann's constant = 1.38066×10^{-23} (J/K), s = collision area (m^2) = 0.42×10^{-18} m^2 for air or N_2, and P is the gas pressure (bar).

Equation (1) remains almost unaffected if we account for velocity distribution effects (e.g. assuming a Maxwell–Boltzmann law of distribution of velocities, see also Kennard 1938). However, if we assume that gas molecules behave like elastic spheres we must account for the persistence of molecular velocities at a collision between two molecules of equal mass. Then Eq. (1) becomes, $D \cong \frac{1.8}{3}\lambda\bar{u}$ (Jeans 1925; Kennard 1938). Finally, Maxwell–Stefan (M–S) theory predicts the following expression for self diffusivity of an ideal gas:

$$D = \frac{2}{3}\lambda\bar{u} \tag{3}$$

Previous studies have shown that Eq. (3) give results that are in good agreement with experiments.

2.3 Estimation of binary diffusion coefficients

Binary diffusion in a gas mixture of species A and B, is obviously more complicated than self-diffusion due to the interaction of the two species in the mixture. Early theories by Meyer that use simplistic extensions of Eq. (1) for the case of binary mixtures, suggest a strong dependence of binary diffusivity, D_{AB}, on concentration of either species in the mixture (Jeans 1925). However, if one accounts for velocity persistence after collisions, then the respective formula for D_{AB} shows little dependence on concentration (Jeans 1925). According to the M–S theory, D_{AB}, is independent of the mixture composition. Experiments, on the other hand, have revealed a good agreement with the M–S theory (Jeans 1925; Hirschfelder et al. 1949; Marrero and Mason 1972; Reid et al. 1987).

A more sophisticated approach, still based on the kinetic theory of gases, is to solve Boltzmann's equation at some special conditions. Thus, at low to moderate pressures, Chapman and Enskog independently derived the following equation:

$$D_{AB} = \frac{0.00266T_g^{3/2}}{PM_{AB}^{1/2}\sigma_{AB}^2\Omega_D} = \frac{0.00188T_g^{3/2}}{P\sigma_{AB}^2\Omega_D}\left[\frac{1}{M_A}+\frac{1}{M_B}\right]^{1/2} \quad (4)$$

where

$$M_{AB} = 2\left[\frac{1}{M_A}+\frac{1}{M_B}\right]^{-1} \quad (5)$$

With P, pressure in bar, T_g, temperature in K, $\sigma_{AB} = (\sigma_A + \sigma_B)/2$, Lennard-Jones collision diameters obtained from viscosity experiments in the gas, Ω_D a diffusion collision integral, which is normally provided as a function of the dimensionless temperature, $T^* = kT_g/\varepsilon_{AB}$ (Neufeld et al. 1972). Note that $\varepsilon_{AB} = \sqrt{\varepsilon_A\varepsilon_B}$, ε_A, ε_B, being characteristic LJ energy minima.

Besides approximate theories, there are several semi-empirical formulas that predict binary diffusivities with good accuracy. Wilke and Lee (1955) have proposed the following semi-empirical formula to estimate D_{AB}:

$$D_{AB} = \frac{\left[3.03 - 0.98/\left(M_{AB}^{1/2}\right)\right](1\times10^{-3})T_g^{3/2}}{PM_{AB}^{1/2}\sigma_{AB}^2\Omega_D} \quad (6)$$

Fuller et al. (1966) have proposed the following formula for D_{AB}:

$$D_{AB} = \frac{0.00143T_g^{3/2}}{PM_{AB}^{1/2}\left[\left(\sum_v\right)_A^{1/3}+\left(\sum_v\right)_B^{1/3}\right]^2} \quad (7)$$

where $\sum_v$ is found for each component by summing atomic diffusion volumes. For N_2 $\sum_v = 18.5$ and for O_2 $\sum_v = 16.3$. Detailed values for all basic elements or simple molecules are provided in any classic text-book on transport phenomena (see for example, Reid et al. 1987).

Equations (6) and (7) give estimations of D_{AB} with average errors around 4–5 % .

2.4 Comparison of self and binary diffusivities for N_2/O_2 mixtures

We have used the above equations to determine self and binary diffusion coefficients for N_2/O_2 mixture at $T_g = 300$ K and $P = 1.5$ bar, where we have experimental diffusivity results for this gas mixture (Hirschfelder et al. 1949).

Looking at the results of Table 1, we observe that all equations give a very good estimate of the experimental diffusivities. Wilke-Lee's expression is in closest agreement with the experiment for the case of binary diffusion. Furthermore, N_2 self-diffusivities are almost identical to binary diffusivities due to the similarities in molecular weights and Lennard-Jones parameters for N_2 and O_2. This important preliminary conclusion allows us to study N_2 self-diffusion and predict the value of N_2/O_2 mixture diffusivity, with negligible error.

2.5 Microscopic simulation of self diffusion in a porous medium

Microscopic simulation of self or tracer diffusion on off-lattice and/or on-lattice 3D structures, has been successfully performed over the last three decades employing Monte Carlo random-walk methods (Evans et al. 1980; Akanni et al. 1987; Torquato and Kim 1989; Reyes and Iglesia 1991; Tassopoulos and Rosner 1992; Melcote and Jensen 1992; Tomadakis and Sotirchos 1993; Vignoles 1995; Burganos 1998; Kainourgiakis et al. 1999; Zalc et al. 2004; Berson et al. 2011). These methods help us determine self-diffusivities at any value of the Knudsen number, Kn, defined as the ratio of the mean free path to the hydraulic diameter of the material:

$$Kn = \frac{\lambda}{d_h} \quad (8)$$

The hydraulic diameter of the structure, d_h, has been already defined in part I of this series, and it is proportional to the ratio of the porosity of the material, ε, over its surface area per unit volume, S_v (Underwood 1970):

$$d_h = \frac{4\varepsilon}{S_V} \quad (9)$$

The above quantity is another measure of the mean pore size of the material and is also equal to the mean intercept or mean pore chord length, $\langle l_p \rangle$, since it corresponds to the mean length of the segments of a randomly drawn line in the pore space of the medium (Torquato 2002). If $Kn \gg 1$ then the mean free path of the molecules, λ, is much higher than the characteristic size of the pores, which means that the molecules prefer to collide with the solid walls almost exclusively (Knudsen regime). This is a case that occurs at very dilute gas densities, or, equivalently, very low pressures, for a given pore diameter. An equivalent way to establish the condition that $Kn \gg 1$, is by having very small pores at a given pressure as can bee seen from Eq. (8). Note that Knudsen diffusion does not depend on pressure. On the other hand, if $Kn \ll 1$, the gas molecules prefer to collide with each other and occasionally collide with the solid walls of the macropores (pure molecular diffusion regime). In this case the ratio of pore diffusivity over its value at the same temperature and pressure conditions, in the free space, remains constant with the

Table 1 Self and binary diffusion coefficients for N_2/O_2 mixture at 300 K and 1.5 bar

	D_{AB} (Eq. 4) (m^2/s)	D_{AB} (Eq. 6) (m^2/s)	D_{AB} (Eq. 7) (m^2/s)	D_{AB} experiment (m^2/s)
O_2-self	1.32×10^{-5}	1.42×10^{-5}	1.32×10^{-5}	–
N_2-self	1.38×10^{-5}	1.48×10^{-5}	1.43×10^{-5}	1.4×10^{-5}
N_2/O_2	1.36×10^{-5}	1.46×10^{-5}	1.39×10^{-5}	1.5×10^{-5}

Experimental values are taken from Hirschfelder et al. 1949

Knudsen number, *Kn*, and hence with pressure. Typically a value $Kn \sim 5 \times 10^{-3}$ ensures that we are in the pure molecular diffusion regime (Burganos 1998).

At the end of the simulation process, the value of self or tracer diffusivity, D, is determined from the mean-square displacement $\langle \xi^2 \rangle$, of a statistically sufficient number of identical molecules injected in the void space of the medium, according to the well known Einstein's equation (Einstein 1926; Chandrasekhar 1943):

$$D = \lim_{t \to \infty} \frac{\langle \xi^2 \rangle}{6 \cdot t} \tag{10}$$

where t is the travel time of the molecules. This quantity is monitored through the distance travelled by the molecules during the simulation, assuming that they move at a constant speed equal to the thermal speed, $\bar{u}$, as indicated in similar studies (see for example Kainourgiakis et al. 1999, and references cited there in). The travel time has to be large enough to ensure that the molecules "feel" the effect of all the structural details of the porous medium, in determining the macroscopic diffusivities. In this sense, the material can be considered as macroscopically homogeneous in terms of its structural and diffusion characteristics.

In order to simulate diffusion at any value of the Knudsen number, *Kn*, we adopt the following step-by step random walk procedure for a large number of inert, point-like molecules: First, a random position in the pore space is defined as the initial position of a point-molecule to travel within the porous medium. Subsequently, direction angles are randomly assigned to the molecule which starts its random walk moving from point to point along this direction, until it collides with another molecule at a distance λ_i, sampled from an exponential distribution with mean, λ (Jeans 1925; Kennard 1938):

$$\lambda_i = -\lambda \exp(\chi),\ \chi \text{ uniform } \in (0, 1) \tag{11}$$

At each step a check is made whether the molecule hits a solid wall before it collides with another molecule, and if the former happens it undergoes a diffuse reflection according to the cosine law (Greenwood 2002). At all times a test is made to determine whether the molecule reaches the boundaries of the 3D medium. Periodic boundary conditions are employed in the present study and two sets of coordinates have been used: local coordinates of the molecule inside the medium and the global ones used for the computations of the total displacements (Burganos 1998; Kainourgiakis et al. 1999). Evidently, for $\lambda \to \infty$ we determine Knudsen diffusivity while for very small λ the algorithm provides the molecular diffusion coefficient. The random walk process described above is illustrated schematically in Fig. 1.

Using the expression from Eq. (1) for pure molecular diffusion in the free phase, $D = D_b = \frac{1}{3}\lambda\bar{u}$ (solution from kinetic theory for molecular diffusion in the absence of velocity persistence after each collision) one can non-dimensionalize pore diffusivity as follows [substituting also $t = s/\bar{u}$ in Eq. (10)]:

$$\frac{D}{D_b(\lambda)} = \lim_{s/\lambda \to \infty} \frac{\langle \xi^2/\lambda^2 \rangle}{2s/\lambda} \tag{12}$$

The standard computational procedure, when tested in a pure unbounded domain ($\varepsilon = 1$) with no solid-wall collisions, predicts that $D/D_b \sim 1$. In other words, the

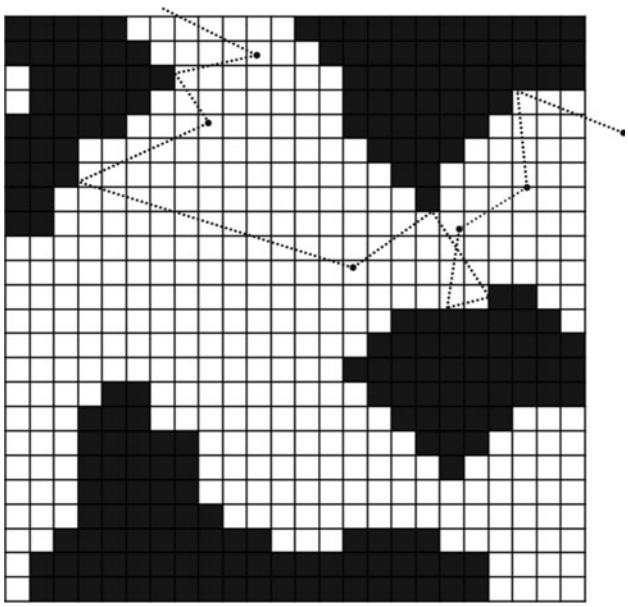

Fig. 1 An illustrative example of the step-by-step random walk process of point tracers in a lattice domain (pore space is drawn in *white* and solid phase in *dark grey*). Note that the random walk process is performed off-lattice (i.e. anywhere) in the domain

current simulation method predicts that in an open domain, $D = D_b = \frac{1}{3}\lambda\bar{u}$. At $P = 1.5$ bar and $T_g = 300$ K, and using the expressions for $\bar{u}$ and λ, already defined in Sect. 2.1, the N_2 self-diffusivity in the bulk phase predicted by Eq. (1) will be $D_b \sim 7.4 \times 10^{-6}$ m^2/s, which is about half the experimental value of D_b for N_2 self or binary diffusion at these conditions (see also Table 1).

The reason for this discrepancy can be found from the fact that in the simulations we have employed no-memory random walks. In other words we have assumed that after an intermolecular collision, all directions of the bouncing molecule are equally probable. However, this is not true as it has already been discussed above introducing the concept of persistence of velocities between molecular collisions, where we have observed a moderate tendency for a succeeding path to favor the general direction of the preceding one.

Because the difference in bulk diffusivities with and without inclusion of molecular persistence of velocities is quite large, it is important to explore whether the assumption of no memory random walk can be relaxed and what effect this might have in the predictions of diffusivities.

2.6 A biased random walk method to account for persistence of velocities

In order to relax the assumption of no-memory random walks, we have followed the idea proposed in the work of Tomadakis and Sotirchos (1993). These authors performed biased random walk simulations by bounding the minor angle ω formed by the vectors representing the directions of a molecule before and after an intermolecular collision through the constraint, $0 \le \omega \le \omega_{\max}$. Evidently if $\omega_{\max} = \pi$, then the molecule is free to scatter freely everywhere in an imaginary sphere centered around the molecule's position at the point of the collision with other molecules. If $\omega < \pi$ then the post-collision direction of the molecule is restricted accordingly. For example if $\omega_{\max} = \pi/2$, then the molecule can scatter freely only in the positive hemisphere formed normal to the molecule's direction before the collision, with center again the point of inter-molecular collision, and so on. The above cases are illustrated in Fig. 2.

Based on the above arguments we have developed biased random walk simulators where we have achieved persistence of the velocities by arbitrarily setting $\omega_{max} \le \pi$. Simulations were performed for an unbounded domain (free space) in order to select the appropriate value for ω_{max} that matches the correct prediction for molecular self-diffusivity in the bulk phase. Results for different ω_{max} values are shown in Fig. 3.

From the above results it is seen that using a value of $\omega_{\max} = \pi/2$ results in a prediction of $D_b \sim 2D_{b,0}$ or $D_b = (2/3)\lambda u_0 \sim 1.5 \times 10^{-5}$ m^2/s. Thus we can predict the experimental self-diffusivity of N_2 in the bulk phase if we consider that there is a persistence of molecular velocities, such that the molecules after an intermolecular collision can only scatter in the positive hemisphere formed normal to the direction of the molecule before the collision and with its center at the point of collision.

Hence, in the present study we employ a biased random walk method with $\omega_{\max} = \pi/2$ to calculate N_2 pore diffusivity at any finite value of the Knudsen number, Kn, as determined by the experimental conditions (mean free path and hydraulic diameter of the material). For the case of Knudsen diffusion where only molecule-wall collisions are

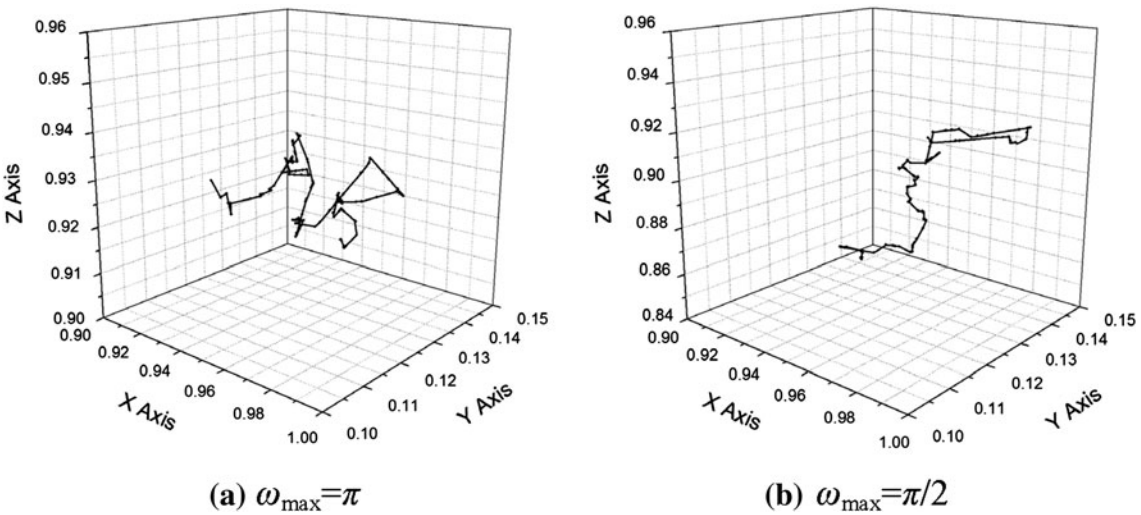

Fig. 2 Molecular trajectories in an unbounded domain, **a** when there is no persistence of molecular velocities and, **b** when there is a persistence of molecular velocities

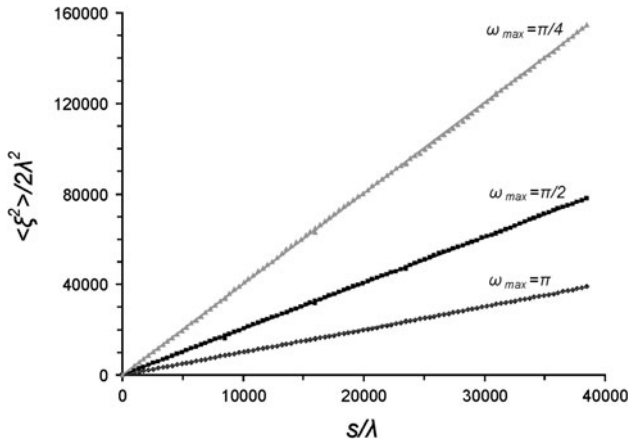

Fig. 3 Mean square displacement versus distance using different bounds of angle ω for random walk simulations of molecular diffusion in the free space ($\varepsilon = 1$)

observed, there should be no effect of velocity persistence between molecular collisions, since the latter do not occur in this case. Furthermore, for the case of pore diffusion at the pure molecular diffusion regime ($Kn \ll 1$) we can still use the standard unbiased random-walk method, since we know that at these conditions the ratio D/D_b reaches a plateau value, which remains constant if we further decrease Kn. Thus, if we use the correct "experimental" value of diffusivity in the free space, D_b, we will get the proper value of pore diffusivity, D. Of course we can also use the biased random walk method using the kinetic theory result for D_b (Eqs. (1) and (12)) and get the correct value for D.

2.7 Estimation of tortuosity

The tortuosity factor or tortuosity, τ, is an empirical parameter that is used to describe the longer connecting paths due to the complexity of the porous structure compared to the motion in the unconstrained free space ($\varepsilon = 1$). Tortuosity can be defined from the following equation:

$$D_p = \frac{\bar{D}}{\tau} \tag{13}$$

where D_p is pore diffusivity for N_2 and does not have imbedded in it the porosity of the material (in accord with its definition in the patent by Ackley and Leavitt 2002) and $\bar{D}$ is a reference diffusivity for N_2, typically determined by Bosanquet's equation (see also, Zalc et al. 2004; Berson et al. 2011):

$$\bar{D} = \left(\frac{1}{D_b} + \frac{1}{D_K}\right)^{-1} \tag{14}$$

where D_b is N_2 bulk or molecular diffusivity in the free space and D_K is the respective Knudsen diffusivity for a capillary with a diameter equal to the hydraulic diameter of the porous material, d_h, or, equivalently, the mean pore chord length, $\langle l_p \rangle$:

$$D_K = \frac{1}{3} d_h \bar{u} = \frac{1}{3} \langle l_p \rangle \bar{u} \tag{15}$$

Previous studies have demonstrated that tortuosity factors defined by Eqs. (13) and (14) show significant dependence on the Knudsen number, despite their purely geometric nature (see for example, Tomadakis and Sotirchos 1993; Zalc et al. 2004). More specifically, tortuosities in the Knudsen regime are often much larger than those measured on the pure molecular diffusion regime. Zalc et al. (2004) have attributed this inconsistency to the inappropriate definition of the reference Knudsen diffusivity, at least for pore structures that are well above their percolation threshold. Furthermore, these authors have shown that tortuosity factors computed in simulated structures made by random sphere packs and spherical aggregates that are well above their percolation threshold, can become independent of the Knudsen number, Kn, if the reference Knudsen diffusivity is defined by Derjaguin's expression (Derjaguin 1946):

$$D_K = \frac{1}{3} \langle l_p \rangle \bar{u} \left[\frac{\langle l_p^2 \rangle}{2 \langle l_p \rangle^2} - \beta \right] \tag{16}$$

where the term $\beta = -\sum_{j=1}^{\infty} \langle \cos \gamma_j \rangle$ describes the nature of the redirecting collisions, through the average cosine of the angles γ_j between trajectory segments separated by j wall collisions. For exponential pore chord length distribution functions (usually met in random sphere packs) it is known that $\frac{\langle l_p^2 \rangle}{2 \langle l_p \rangle^2} = 1$. Furthermore, Derjaguin has shown for molecules striking randomly placed spheres using Knudsen's cosine law that $\beta = 4/13$. (Derjaguin 1946). So we can consider an idealized case of a random sphere pack, which in this case predicts a Knudsen diffusivity of the form:

$$D_K = \frac{3}{13} \langle l_p \rangle \bar{u} \tag{17}$$

The above expression can be used to compute the reference diffusivity $\bar{D}$, in Eq. (14).

2.8 Mercury porosimetry

2.8.1 Mercury intrusion

Mercury (Hg) porosimetry is by far the most popular method for characterizing porous materials with pores in the range of $\sim$100 μm down to $\sim$0.003 μm (Lowell and

Shields 1991; Leon and Leon 1998; Rouquerol et al. 2012). Compared to alternative characterization methods such as gas sorption, Hg porosimetry covers a much wider pore size range, while it is based on simpler physicochemical principles and it is much faster in operation. Nevertheless, Hg porosimetry has some important limitations that must be taken into account when analyzing the structure of porous materials particularly when there is no additional/complementary information from other characterization techniques, such as microscopy, tomography, small and very small angle scattering, etc.

The most commonly used experiment in Hg porosimetry consists of increasing the pressure in small steps and measuring the resulting Hg entering the sample, after allowing the system to reach equilibrium at each step. This experiment is called Hg-intrusion. Hg-intrusion is normally followed by the reverse process called Hg-retraction or extrusion. The most important limitations of the Hg-intrusion when applied to extract pore size distribution of a porous material is that it is based on the assumption that the porous matrix can be represented by a bundle of cylindrical pores. This assumption has some major limitations:

The Washburn equation used to relate applied hydraulic pressure with pore radius has been developed on the assumption of cylindrical pores in shape:

$$P = \frac{-2\gamma\cos(\theta)}{r} \tag{18}$$

where P is the pressure required to fill with Hg a cylindrical pore of radius r, γ is the surface tension of Hg in air at ambient temperature, and θ is the contact angle of Hg at the pore surface. For wetting liquids $\theta < 90°$, while for non-wetting liquids such as Hg, $90° < \theta \leq 180°$. For a purely spherical Hg meniscus $\theta = 180°$, while for Hg in contact with zeolite surfaces this value is measured to be around 135°. Evidently, non-wetting liquids like Hg must be hydraulically forced to fill the pores of the material. The applied pressure ranges from very small pressures to fill pores with a radius of around 100 μm and up to very high pressures in the order of 60,000 psia for intrusion of pores with a radius of $\sim$0.003 μm. Note that at high pressures compressibility effects must be also taken into account.

In extracting pore size distributions during Hg intrusion, we assume that all pores are equally accessible to the exterior Hg reservoir. This assumption can only be met if we represent the pore structure in the form of a bundle of capillaries or if pore connectivity, n_T, is very high ($n_T \rightarrow \infty$). In reality however, pore network effects can be quite important resulting in the so-called pore shadowing or ink-bottle phenomenon where a large pore has smaller entrances that connect it with the Hg reservoir and can only be filled at a pressure, P, higher than that required by its actual (inner) dimensions. A schematic illustration of the pore shadowing effect during Hg-intrusion in idealized porous media is presented in Fig. 4. The idealized porous medium is made of three cylindrical pores connected in series ($n_T = 2$). Two different cases are considered: In the first case, the inner pore is connected to larger entrance pores (Fig. 4a, b), while in the second case, the inner pore is connected to smaller entrance pores (Fig. 4c, d). It is seen that when the inner pore is smaller than either of the two entrance pores, Hg intrusion predicts the correct pore size distribution (Fig. 4a, b). On the other hand, when the inner pore is larger than both entrance pores, the predicted pore size distribution is biased towards smaller than actual pore sizes (Fig. 4c, d). Thus, capillary network models must be employed to determine additional structural properties including, network connectivity and pore

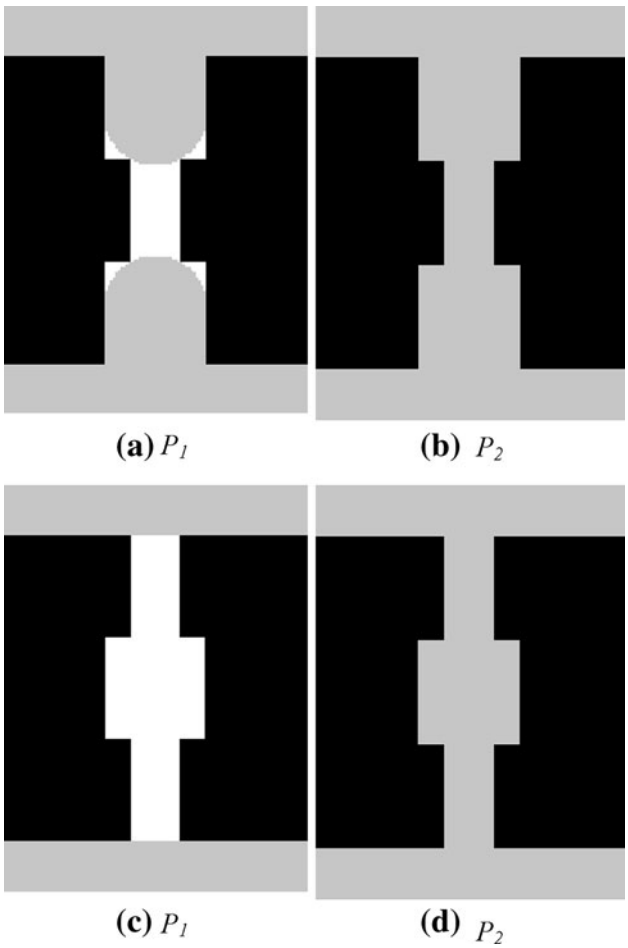

Fig. 4 Schematic illustration of the pore shadowing effect during Hg-intrusion in idealized porous media made of cylindrical pores with radii r_1 and r_2 at pressures P_1 and P_2 respectively ($r_1 > r_2$ and $P_1 < P_2$). 2D cuts are shown with solid phase in *black*, pore space in *white* and Hg in *gray* color. When the inner pore is smaller than either of the two entrance pores, Hg intrusion predicts the correct pore size distribution. When the inner pore is larger than both entrance pores the predicted pore size distribution is biased towards smaller than actual pore sizes

correlations and also describe complex hysteresis phenomena occurring during the complete cycle of Hg intrusion-retraction. Such models of varying complexity have been used over the past three decades and have been often quite successful in providing structural characteristics of the porous materials examined (Androutsopoulos and Mann 1979; Portsmouth and Gladden 1991; Tsakiroglou and Payatakes 1990, 1991, 1998; Ioannidis and Chatzis 1993; Mata et al. 2001; Čapek et al. 2007).

Pore shadowing during Hg-intrusion can have important implications when developing porous materials for different physicochemical applications including gas separations and heterogeneous catalysis. Thus for example if we define the median pore diameter, d_m, as that where 50 % of the total pore volume of the material is accessed, it is obvious that this diameter, when calculated by Hg intrusion, includes pore space accessibility effects that are also crucial in many transport process including molecular diffusion and flow. In other words d_m calculated by Hg intrusion may be biased towards smaller than actual pore sizes, which should affect the correct mass transport characteristics of the material. In essence d_m calculated by Hg intrusion contains implicit information on the pore network connectivity of the material. Thus it is evident that two porous materials with the same value of d_m, may exhibit different mass transfer characteristics simply because this value may or may not be biased by pore shadowing effects.

Note that Hg-retraction experiments can also be used to extract structural information. However such experiments are also limited by additional accessibility-based phenomena that result in several complications including contact angle hysteresis, Hg entrapment, much longer relaxation times towards equilibrium, etc. (Salmas and Androutsopoulos 2001; Rigby and Edler 2002; Rigby et al. 2008; Thommes et al. 2008). For these reasons Hg-retraction curves are not used on a routine basis for pore size distribution calculations, although they may include important structural information particularly when combined with the respective intrusion curves (Portsmouth and Gladden 1991; Mata et al. 2001). Note that Hg-porosimetry can be also employed to estimate tortuosity factors (Cagnilia 1986).

2.9 Simulation of Hg-porosimetry by a full-morphology method

There have been several attempts to simulate Hg-intrusion porosimetry on 3D lattices:

(a) Pure morphology models. These are purely morphological in nature and do not involve any physics or chemistry, while the shape of the menisci is assumed to be spherical ($\theta = 180°$). There exist several publications in the open literature dealing with the simulation of Hg-intrusion or similar phenomena such as drainage in totally wetting porous media (Garboczi and Bentz 1991; Hazlett 1995; Hilpert and Miller 2001; Schulz et al. 2007). These models are relatively simple to develop, and can access large pore structures at a high speed. Their main limitation is that they are purely geometric in nature and assume completely spherical interfaces. Nevertheless, they have been shown to represent satisfactorily experimental intrusion curves (Hilpert and Miller 2001).

(b) Lattice gas and/or density functional theory (DFT) models. These models have been developed by Monson and co-workers (Porcheron and Monson 2004; Porcheron et al. 2005, 2007), utilizing the same concepts from Statistical Mechanics used to simulate capillary condensation in mesoporous structures. They can capture many of the qualitative aspects of Hg-porosimetry.

(c) Lattice Boltzmann Equation (LBE) methods. These methods can be used to simulate two phase flows in porous media, so they can be adopted to simulate Hg intrusion (Hyväluoma et al. 2004; Vogel et al. 2005; Thommes et al. 2009). In general, LBE methods can be very effective and simulate complex physicochemical processes qualitatively and in certain case quantitatively too. Nevertheless, these methods are still very expensive computationally, particularly if we want to simulate Hg intrusion over large pore structures and/or with high space resolution.

The mercury porosimetry simulation method (MP) used in the present study belongs to class (a), as it is purely morphological in nature. The MP simulation algorithm has been developed in two and three dimensions as follows:

To begin mercury intrusion simulation, the digitized porous domain is surrounded with mercury by classifying all pixels within a fixed distance from the box outer surfaces as active mercury. These pixel locations are stored in an array as the active locations for mercury invasion. Intrusion is simulated by creating a flow field at each of the active mercury locations. Assuming a contact angle of 180° between mercury and porous medium, the flow field can be represented as a circle in two dimensions or a sphere in three dimensions of a fixed diameter d. This value of contact angle is not realistic for most porous materials where this value is between 120° and 140°. However, the exact value of the contact angle used in this work is not important, since according to Eq. (18), the $\cos(\theta)$ term is only a scale factor that appears in the relation between intrusion pressure and pore size. If a circle or sphere, of diameter d, can be centered at an active mercury location without overlapping any solid material, all pixels that it

encompasses and still belong to the empty pore space are reclassified as active mercury. Accordingly, their locations are stored in a new array. Following this flow propagation step, all originally active pixels are changed to deactivated mercury. After all flow fields from the original active mercury array have been processed, the procedure is repeated for the new active array. This iterative process continues until there are no new flow fields to explore, and the new active mercury array is empty. At this point all the area of the pore structure accessible by mercury from the exterior, for a flow diameter d, have been identified. The procedure is continued by progressively decreasing d, until the total pore volume is completely intruded or until the size of d reaches its minimum value (1 or 2 pixels depending on the way we define a digitized circle or sphere, see also Hilpert and Miller 2001).

A schematic illustration of the MP simulation in two dimensions is presented in Fig. 5 for Hg intrusion in a random disc pack made by cutting a 2D slice from a random sphere pack. Note that the pore shadowing effect is much more pronounced in two dimensions compared to three dimensions due to the obvious smaller number of degrees of accessibility as we reduce dimensions in space.

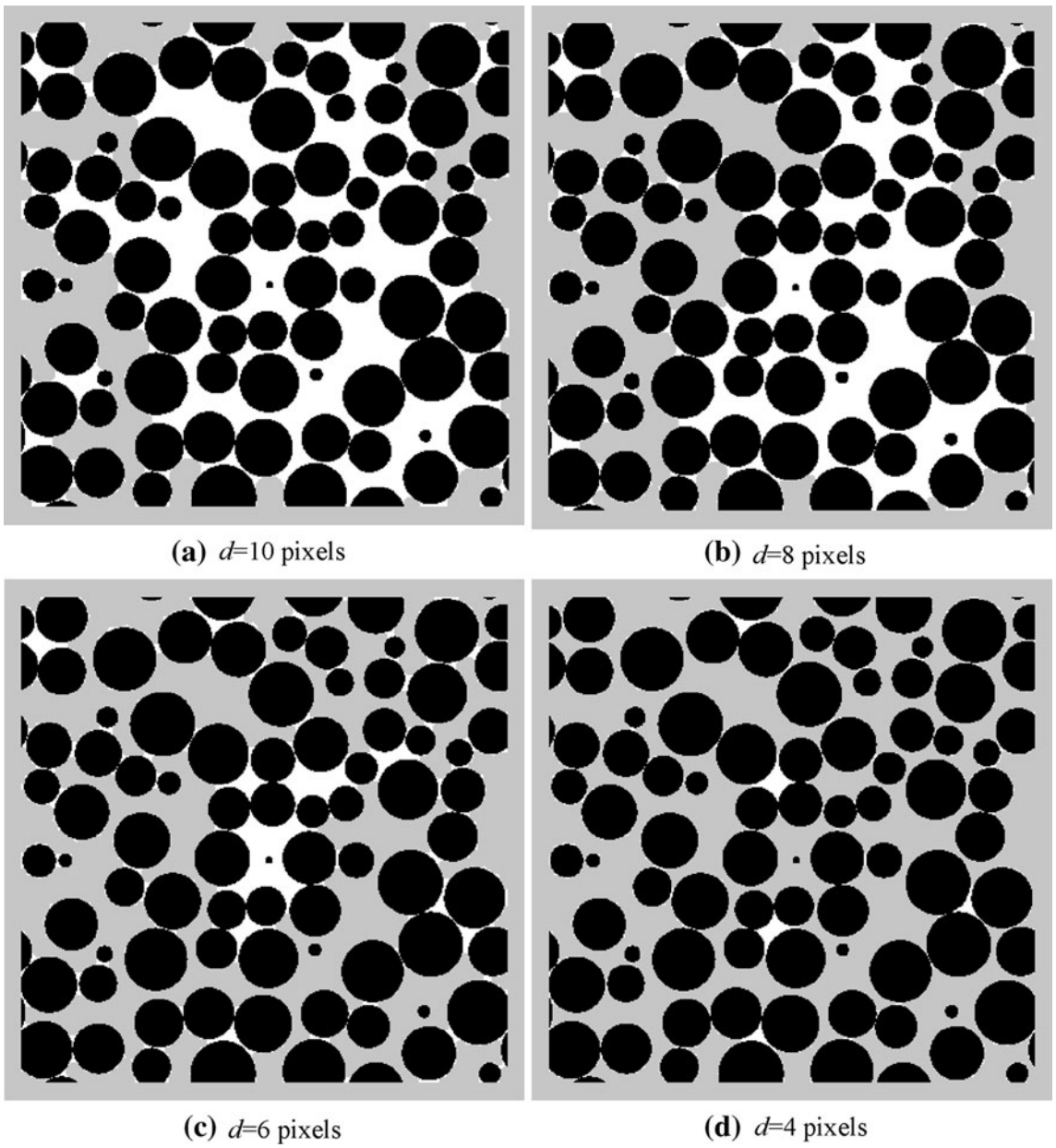

Fig. 5 Schematic illustration of MP simulation in 2D based on a pure morphological model. Solid phase is in *black*, pore space is in *white* and Hg is in *gray* color

The simulation algorithm described above has some distinct differences with the actual intrusion experiment. In a mercury intrusion experiment, the pressure is directly measured and the intruded pore diameter is extracted using Eq. (18). In our simulation, the pore diameter being intruded is fixed by our choice of the diameter of the mercury circle or sphere we try to place inside the porous medium. Hence, there is no need to use Eq. (18), since intrusion pressure does not come into the algorithm at all.

It should be noted that the present intrusion simulation algorithm has a different assessment in two and three dimensions. In two dimensions it is justified to have circular mercury meniscus in the completely non-wetting limit, since there is only one radius of curvature to be fixed by the mercury's surface tension and the applied pressure. However, in three dimensions the meniscus shape does not have to be spherical as in this case it is the sum of two radii of curvatures that is fixed by the surface tension and applied pressure. So if mercury spheres are used to implement the MP algorithm in three dimensions, the volume intruded at a given pore diameter will only be a lower bound, as a pore that will not admit a sphere of that diameter might very well admit a different shape that also satisfies the meniscus curvature equation. Nevertheless, the information from such a simulation model can be still very useful, in the sense of a lower bound. For the scope of the present study we will focus on the simulation of Hg intrusion assuming spherical menisci during intrusion.

3 Results and discussion

3.1 Pore diffusion

Diffusion simulation studies have been performed at reconstructed 3D domains of each of the three beads of the zeolite adsorbent examined, as well as on a reconstructed domain made using average statistical input, namely, porosity and two point correlation function. All these reconstructions have been developed in part I of these series using standard and hybrid SA methods (Kikkinides and Politis 2013). The adsorbent examined is a binderless zeolite agglomerate made using kaolin or kaolin-type clays as binders and subsequent caustic digestion (CD) to convert the clay to zeolite after bonding (Chao and Pontonio 2002) and has improved mass transfer characteristics (Chao and Pontonio 2002; Ackley et al. 2003). Simulations typically involved a large number of 4,000–8,000 test molecules and dimensionless simulation times of the order of 1–2 $\times$ 10^7, that ensure a sufficiently large number of molecule-wall collisions of the order of 50,000–100,000 even at low Knudsen numbers. The results from the diffusion simulations are summarized in Table 2 where we have also included for comparison the experimental value measured on the particular zeolite adsorbent (Ackley et al. 2003).

Table 2 Summary of diffusion simulations ($T_g = 300$ K, $P = 1.5$ bar)

Sample	Porosity ε	D_{N2} (m^2/s)	
		Standard SA	Hybrid, $T = 1 \times 10^{-10}$
Reconstructed sample of bead 1	0.320	1.78×10^{-6}	4.04×10^{-6}
Reconstructed sample of bead 2	0.330	2.33×10^{-6}	4.41×10^{-6}
Reconstructed sample of bead 3	0.315	1.73×10^{-6}	3.96×10^{-6}
Averaged values	0.322	1.95×10^{-6}	4.14×10^{-6}
Reconstructed sample with average statistical input	0.322	2.20×10^{-6}	4.25×10^{-6}
Experiment	0.379	4.20×10^{-6}	

It is seen that N_2 molecular diffusivity values of the 3D structures generated with the hybrid SA method using an initial temperature, $T = 1 \times 10^{-10}$, are in excellent agreement with the experimental diffusivity measurements. More particularly, if we consider the diffusivity value of the reconstructed domain based on the average statistical input, we observe a pore diffusivity of 4.25×10^{-6} m^2/s, which has a small relative error of 1.2 % when compared to the experimental value of 4.2×10^{-6} m^2/s. The diffusivity predictions based on the 3D structures generated with the standard SA method, on the other hand, produce a pore diffusivity of 2.20×10^{-6} m^2/s, which gives a high relative error of 47.6 %, compared to the experimental value. Similar behavior is observed when comparing each of the three beads examined in this study. The results from pore diffusion simulations imply that the structure generated by the hybrid method reproduces much more accurately the macroporous architecture of the zeolite adsorbent agglomerate compared to the structure made by the standard SA method and are in accord with the conclusions drawn in Part I of this series, based on the chord length distribution measurements on these structures. To elaborate further on this, we have performed pore diffusion simulations on structures made by the hybrid method using an initial temperature, $T = 1 \times 10^{-8}$. The resulting N_2 pore diffusivity for the case of a 3D replica based on the average statistical input is found to be 2.70×10^{-6} m^2/s, which gives a relative error of 35.7 %, compared to the experimental value. We have seen in part I that this structure has improved matching in chord length distribution functions compared to the one made by the standard SA method, but

it still less accurate compared to the structure made with the hybrid method using an initial temperature, $T = 1 \times 10^{-10}$. The results from the diffusion simulation studies are in accord with the above conclusion. Thus, it follows that as we improve our matching of pore and (more importantly) mass chord length distribution functions, we also improve our matching in N_2 pore diffusivities. This important conclusion that pore and mass (solid) chord length distribution functions seem to significantly affect the value of transport properties of a porous material, has been previously suggested for the case of Knudsen permeation is alumina porous plugs (Kainourgiakis et al. 2000). Our present findings support further this important conclusion. Although we cannot prove that chord length distribution functions control exclusively the value of pore diffusivity, we can argue that matching both pore and mass chord length distribution functions is a necessary (though probably not sufficient) condition for accurate structural representation.

3.2 Effect of pressure on pore diffusivity

After validating the 3D structure produced by the hybrid SA method, we extend our diffusion simulations at various pressures to study the dependence of N_2 pore diffusivity on pressure (and hence Knudsen number). This dependence is important when evaluating adsorbents for PSA-VSA-VPSA processes, where pressure varies from super- to sub-atmospheric values, depending on the specific process employed. The results from simulations on reconstructed domains made by the hybrid SA method ($T = 1 \times 10^{-10}$) using average statistical input, are presented in Fig. 6.

It is seen that at high pressures molecular diffusion predominates and pore diffusivity is inversely proportional to pressure as expected even from Eqs. (4), (6), (7), that predict molecular diffusivities for binary mixtures in the free space. At very low pressures, on the other hand, Knudsen diffusion controls mass transfer and pore diffusivity is almost independent of pressure. In the same figure we have plotted pore diffusivity predictions based on Bosanquet's expression:

$$\frac{1}{D_p} = \frac{1}{D_{p,b}} + \frac{1}{D_{p,K}} \tag{19}$$

In the above equation D_p is pore diffusivity at a pressure P, $D_{p,b}$ is the expression for pore diffusivity in the pure molecular diffusion regime computed at the same pressure, and $D_{p,K}$ is Knudsen diffusivity for N_2. $D_{p,b}$ is determined as follows: First we compute the value of pore diffusivity in the pure molecular diffusion regime that corresponds to a Knudsen number Kn $\sim 5 \times 10^{-3}$. This value is found to be equal to $D_{p,b} = 1.21 \times 10^{-7}$ m^2/s at a pressure of $\sim$34 bar, where the free space diffusivity is $D_b = 3.33 \times 10^{-7}$ m^2/s, so that their ratio is, $\frac{D_{p,b}}{D_b} = 0.363$. Since we know that at the pure molecular diffusion regime, $\frac{D_{p,b}}{D_b}$ is constant, we simply multiply this ratio with the appropriate value of D_b in the free space that corresponds to a pressure P, to determine $D_{p,b}$ at each pressure. The results from Fig. 6, show a very good agreement between the actual simulation diffusivities and those predicted by Bosanquet's equation, confirming the validity of the latter.

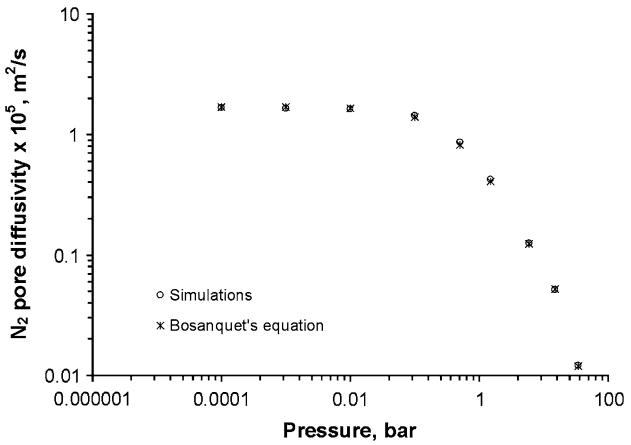

Fig. 6 Effect of pressure on N_2 pore diffusivity, computed on the reconstructed sample with average statistical input, made with the hybrid method

3.3 Estimation of tortuosity

We have employed Eq. (13) to calculate tortuosity, τ. In this equation, the reference diffusivity, $\bar{D}$, has been determined from Eq.(14) with D_K defined by either Eq. (15) or (17). The effect of Knudsen number on τ is shown in Fig. 7 using either choice of D_K. It is seen that tortuosity with D_K defined by Eq. (15) shows significant variation with Kn, particularly in the transition regime going from low to high pressures (from Knudsen to pure molecular diffusion regime, respectively). On the other hand, when Derjaguin's expression for D_K is employed through Eq. (17) this variation almost diminishes, in accord with the findings of Zalc et al. (2004), for the case of more idealized pore structures based on random sphere packs, and Papadopoulos et al. (2007), for the case of ethane diffusion in beds of NaX zeolite crystals. Evidently, the average value of τ for the zeolite adsorbent under study is, $\langle \tau \rangle = 2.68$, with a standard deviation of 0.07. This value is purely geometry dependent and can be safely used to determine pore diffusivity for other gases, at least for cases of self-diffusion and/or binary diffusion of gases with similar molecular weights, kinetic diameters, and other basic physicochemical characteristics.

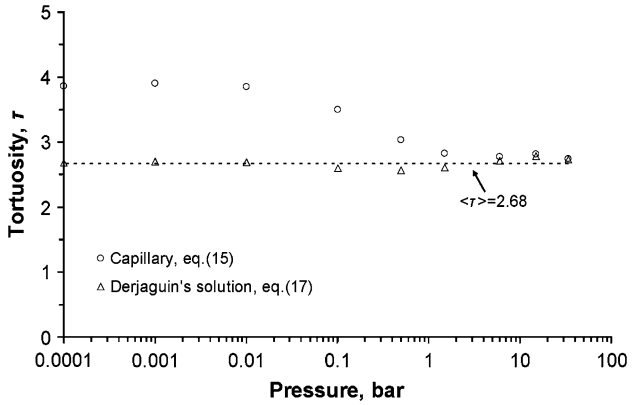

Fig. 7 Variation of tortuosity with pressure, based on diffusion simulations on the reconstructed sample with average statistical input, made with the hybrid method

3.4 Hg intrusion porosimetry

Further to the pore diffusion simulation studies we have simulated Hg-intrusion in the reconstructed images using the pure morphology method outlined in the respective section above. In Fig. 8, we compare simulated Hg-intrusion porosimetry curves measured on reconstructed 3D images made by the standard and the hybrid SA method with $T = 1 \times 10^{-10}$. In the same Figure we have plotted the respective experimental curve measured on the zeolite adsorbent. To be able to make clear comparisons we have normalized all Hg-intrusion curves by the maximum intruded volume in each case. Moreover, we have further treated the experimental Hg-intrusion curve by subtracting at each point the volume intruded at 1 atm and then by normalizing it with the maximum intruded volume minus the intruded volume at 1 atm. This is because at pressures below 1 atm, we intrude pores with sizes of the order of

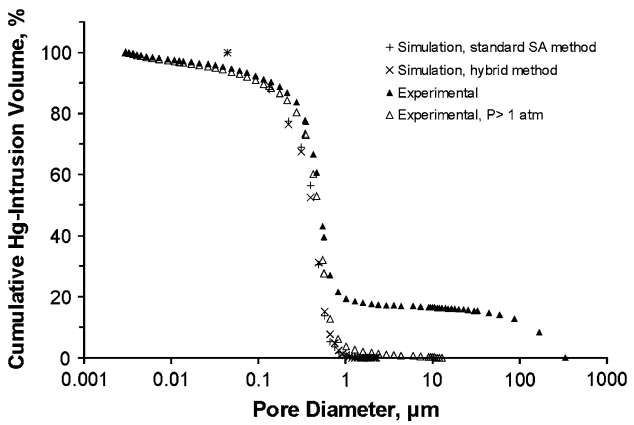

Fig. 8 Simulated and experimental cumulative Hg-intrusion curves for the zeolite adsorbent under study

100 μm or more, which is beyond the range of the SEM micrograph and cannot be detected with our method. Nevertheless, pores of such size are most likely not associated with the internal pore structure of the adsorbent and refer rather to the interstices between zeolite particles or beads, since a sample used from Hg-porosimetry experiments contains a large number of such particles, packed together in the sample container.

Looking at the results in Fig. 8, it is evident that the two simulation curves are in very close agreement with each other and in an overall fair agreement with the experimental Hg-intrusion curve, specifically after the latter is normalized for pressures above 1 atm. As expected, the simulated intrusion volume at a given pore diameter is always lower than its respective experimental value. More specifically the simulation curves significantly underestimate the amount of intruded volume with a relative error of 80–90 % for cumulative intrusion volumes up to 10 %. The error remains quite high (50–70 %) for cumulative intrusion volumes up to 25 %, dropping to 35 % for a cumulative pore volume of ~47 %. For cumulative intrusion volumes of 50 % and up to ~88 % the relative error drops significantly to around 10–13 %. The simulations for either structure predict a median pore diameter around 0.42 μm, which is in very good agreement with the experimental value (0.475 μm). The above differences between simulated and experimental intrusion curves justify our previous suggestion that a Hg-intrusion curve resulting from MP simulations should be considered as a lower bound of the actual experimental curve. Nevertheless, the relative error in the predicted median pore diameter is around 11 %, which is remarkably small, considering the assumptions involved in the MP simulator. Our overall assessment on the MP simulator based on the full morphology method is that it can give a reasonably good description of the process, in a limited region of intrusion volumes between 50 and 88 %.

An additional conclusion drawn when looking at the results of Fig. 8, is that there is almost no difference in the simulated Hg-intrusion curves between the reconstructed domain made with the hybrid and that made with the standard SA method. Given the significant differences obtained in simulated N_2 pore diffusivities on the same structures, it follows that, contrary to chord length distribution functions, Hg-intrusion curves simulated by pure morphological models do not contain sufficient structural information that can distinguish between pore structures with significantly different mass transfer characteristics. Of course this conclusion depends on the ability of the MP simulator to describe accurately the physics of the intrusion phenomenon, which in the present case appears to be reasonably good only in a limited region of intrusion volumes between 50 and 88 %.

The additional use of the Hg-retraction branch is expected to add significant gain in the structural characterization of a macroporous structure, particularly when combined with mesoscopic simulation methods (Rigby et al. 2011). Unfortunately, we have not been able to simulate Hg-retraction with the pure morphology method, as there are several important issues associated with this process, that require additional theoretical development and will be a subject of a future work. Backscattered SEM micrographs, on the other hand, when taken at properly extracted and polished 2D cross sections of the porous material, contain sufficient structural information, in the form of pore and mass chord length distribution functions, that can distinguish among pore structures with different mass transfer rates. Evidently, the direct link between these structural properties and pore diffusivity will provide the necessary route to improve the mass transfer rate of porous adsorbents. It must be emphasized that the SEM sample preparation method is very important in obtaining realistic 2D cross-sections of the actual porous material. For this reason the sample must undergo a series of steps, including, epoxy impregnation, polishing and epoxy surface removal processing before SEM micrographs are obtained. The excellent agreement between simulated and experimental pore diffusion and the fair reproduction of the Hg-intrusion curve by a simplified morphological model, support the above argument. Evidently, additional 3D characterization techniques (Levitz and Tchoubar 1992; Rouquerol et al. 2012) should be employed to measure the basic statistical structural properties and confirm that the obtained SEM micrographs represent realistic 2D sections of the actual porous medium.

4 Conclusions

In part II of the series we complete the evaluation of 3D digitized reconstructions of a binderless zeolite adsorbent with improved mass transfer rates. It is seen that the hybrid SA method with $T = 1 \times 10^{-10}$, which preserves, besides low order correlations, pore and mass chord length distribution functions, predicts the experimental value of N_2 pore diffusivity with a relative error of ~ 1.2 %. The standard SA method, on the other hand, that only guarantees matching of the low order correlations (porosity and two-point correlation function) gives a prediction of pore diffusivity with a relative error of ~ 47.6 %.

Additional studies of N_2 pore diffusion simulations on intermediate structures show that as we improve our matching of experimental pore and mass (solid) chord length distribution functions during the reconstruction process, we also improve matching of the experimental N_2 pore diffusivities. Hence we conclude that matching chord length distribution functions is a necessary (though probably not sufficient) condition for accurate structural representation.

Further to the pore diffusion simulation studies we have simulated Hg-intrusion in the reconstructed 3D images using a pure morphology method. Our findings have shown good agreement of either simulated structure with the experimental curve, when properly normalized, for intrusion volumes in the range of 50–88 %. Moreover, it is seen that standard and hybrid SA methods produce simulated Hg-intrusion curves that are almost indistinguishable. This result suggests that Hg-intrusion porosimetry alone may not be sufficient to extract structural parameters that control pore diffusivity, at least for the type of the zeolite adsorbent structure studied in the present work. However, additional work with more detailed simulation models must be performed to draw a safer conclusion on this matter.

SEM micrographs, on the other hand, when properly obtained to represent realistic 2D sections of the porous material, contain sufficient structural information, in the form of pore and mass chord length distribution functions, that can distinguish among pore structures with different mass transfer rates, with the additional employment of 3D stochastic reconstruction methods. Evidently, the direct link between these structural parameters and pore diffusivity will provide the necessary route to improve the mass transfer rate of porous adsorbents.

Acknowledgments We thank Drs. Mark Ackley, Philip Barrett and Neil Stephenson from Praxair, Inc. for stimulating discussions and for providing us with mercury porosimetry data on the binderless zeolite adsorbent. We also thank Dr. Michael Kainourgiakis for useful discussions on the concept of biased diffusion simulations. Financial support from Praxair, Inc. is gratefully acknowledged.

References

Ackley, M.W., Leavitt, F.W.: Rate-enhanced gas separation. US Patent 6,500,234, 2002

Ackley, M.W., Smolarek, J., Leavitt, F.W.: Pressure swing adsorption gas separation method, using adsorbents with high intrinsic diffusivity and low pressure ratios. US Patent 6,506,234, 2003

Akanni, K.A., Evans, J.W., Abramson, I.S.: Effective transport coefficients in heterogeneous media. Chem. Eng. Sci. **42**, 1945–1954 (1987)

Androutsopoulos, G.P., Mann, R.: Evaluation of mercury porosimetry experiments using a network pore structure model. Chem. Eng. Sci. **34**(10), 1203–1212 (1979)

Berson, A., Choi, H.-W., Pharoah, J.G.: Determination of the effective gas diffusivity of a porous composite medium from the three-dimensional reconstruction of its microstructure. Phys. Rev. E **83**(2), 026310 (2011)

Burganos, V.N.: Gas diffusion in random binary media. J. Chem. Phys. **109**, 6772–6779 (1998)

Cagnilia, S.C.: Construction of the tortuosity factor from porosimetry. J. Catal. **102**(2), 401–418 (1986)

Čapek, P., Hejtmánek, V., Brabec, L., Zikánová, A., Kocirík, M.: Network modelling of capillary pressure curves, permeability, and diffusivity. Chem. Eng. Sci. **62**, 5112–5117 (2007)

Chandrasekhar, S.: Stochastic problems in physics and astronomy. Rev. Mod. Phys. **15**, 1–89 (1943)

Chao, C.C., Pontonio, S.J.: Advanced adsorbent for PSA. US Patent 6,425,940, 2002

Derjaguin, B.: Measurement of the specific surface of porous and disperse bodies by their resistance to the flow of rarified gases. Comptes Rendus (Doklady) de l'Académie des Sciences de l'URSS. 53(7): 623–626 (1946)

Einstein, A.: Investigations on the theory of Brownian motion. Dover, New York (1926)

Evans, J.W., Abbasi, M.H., Sarin, A.: A Monte-Carlo simulation of the diffusion of gases in porous solids. J. Chem. Phys. **72**, 2967–2973 (1980)

Fuller, E.N., Schettler, P.D., Giddings, J.C.: A new method for prediction of binary gas-phase diffusion coefficients. Ind. Eng. Chem. **58**(5), 19–27 (1966)

Garboczi, E.J., Bentz, D.P.: Digitized simulation of mercury intrusion porosimetry. In: Mindess, S. (ed.) Ceramic Transactions, Advances in Cementitious Materials, vol. 16, pp 365–379. American Ceramic Society, Westerville (1991)

Greenwood, J.: The correct and incorrect generation of a cosine distribution of scattered particles for Monte-Carlo modeling of vacuum systems. Vacuum **67**(2), 217–222 (2002)

Hazlett, R.D.: Simulation of capillary-dominated displacements in microtomographic images of reservoir rocks. Transp. Porous Media **20**(1–2), 21–35 (1995)

Hilpert, M., Miller, C.T.: Pore-morphology-based simulation of drainage in totally wetting porous media. Adv. Water Resour. **24**(3–4), 243–255 (2001)

Hirschfelder, J.O., Bird, R.B., Spotz, E.L.: The transport properties of gases and gaseous mixtures. II. Chem. Rev. **44**(1), 205–231 (1949)

Hyväluoma, J., Raiskinmäk, P., Jäsberg, A., Koponen, A., Kataja, M., Timonen, J.: Evaluation of a lattice-Boltzmann method for mercury intrusion porosimetry simulations. Futur. Gener. Comput. Sys. **20**, 1003–1011 (2004)

Ioannidis, M.A., Chatzis, I.: A mixed percolation model of capillary hysteresis and entrapment in mercury porosimetry. J. Colloid Interface Sci. **161**(2), 278–291 (1993)

Jeans, J.H.: The dynamical theory of gases. Cambridge University Press, London (1925)

Kainourgiakis, M.E., Kikkinides, E.S., Stubos, A.K., Kanellopoulos, N.K.: Simulation of self-diffusion of point-like and finite-size tracers in stochastically reconstructed Vycor porous glasses. J. Chem. Phys. **111**(6), 2735–2743 (1999)

Kainourgiakis, M.E., Kikkinides, E.S., Steriotis, T.A., Stubos, A.K., Tzevelekos, K.P., Kanellopoulos, N.K.: Structural and transport properties of alumina porous membranes from process-based and statistical reconstruction techniques. J. Colloid Interface Sci. **231**(1), 158–167 (2000)

Karger, J., Cocirik, M., Zikanova, A.: Molecular transport through assemblages of microporous particles. J. Colloid Interface Sci. **84**(1), 240–249 (1981)

Karger, J., Ruthven, D.M.: Diffusion in zeolites. Wiley, New York (1992)

Kennard, E.H.: Kinetic theory of gases. Mc Graw-Hill, New York (1938)

Kikkinides, E.S., Politis, M.G.: Linking pore diffusivity with macropore structure of zeolite adsorbents. Part I: three dimensional structural representation combining scanning electron microscopy with stochastic reconstruction methods. Adsorpt. J. Int. Adsorp. Soc (2013). doi:10.1007/s10450-013-9544-1

Leon, Y., Leon, C.A.: New perspectives in mercury porosimetry. Adv. Colloid Interface Sci. **76–77**, 341–372 (1998)

Levitz, P., Tchoubar, D.: Disordered porous solids from chord distributions to small angle scattering. J. Phys. I **2**(6), 771–790 (1992)

Lowell, S., Shields, J.E.: Powder surface area and porosity, 3rd edn. Chapman and Hall, London (1991)

Neufeld, P.D., Janzen, A.R., Aziz, R.A.: Empirical equations to calculate 16 of the transport collision integrals $\Omega(l, s)^*$ for the Lennard-Jones (12–6) potential. J. Chem. Phys. **57**, 1100 (1972)

Marrero, T.R., Mason, E.A.: Gaseous diffusion coefficients. J. Phys. Chem. Ref. Data **1**(1), 3–118 (1972)

Mata, V.G., Lopes, J.C.B., Dias, M.M.: Porous media characterization using mercury porosimetry simulation. 2. An iterative method for the determination of the real pore size distribution and the mean coordination number. Ind. Eng. Chem. Res. **40**(22), 4836–4843 (2001)

Melcote, R.R., Jensen, K.F.: Computation of transition and molecular diffusivities in fibrous media. AIChE J. **38**(1), 56–66 (1992)

Papadopoulos, G.K., Theodorou, D.N., Vasenkov, S., Karger, J.: Mesoscopic simulations of the diffusivity of ethane in beds of NaX zeolite crystals: comparison with pulsed field gradient NMR measurements. J. Chem. Phys. **126**(9), 094702 (2007)

Porcheron, F., Monson, P.A.: Modeling mercury porosimetry using statistical mechanics. Langmuir **20**(15), 6482–6489 (2004)

Porcheron, F., Monson, P.A., Thommes, M.: Molecular modeling of mercury porosimetry. Adsorption **11**, 325–329 (2005)

Porcheron, F., Thommes, M., Ahmad, R., Monson, P.A.: Mercury porosimetry in mesoporous glasses: a comparison of experiments with results from a molecular model. Langmuir **23**(6), 3372–3380 (2007)

Portsmouth, R.L., Gladden, L.F.: Determination of pore connectivity by mercury porosimetry. Chem. Eng. Sci. **46**, 3023–3036 (1991)

Reid, R.C., Prausnitz, J.M., Poling, B.E.: The properties of gas and liquids, 4th edn. McGraw-Hill, New York (1987)

Reyes, S.C., Iglesia, E.: Effective diffusion coefficients in catalyst pellets: new model porous structures and transport simulation techniques. J. Catal. **129**, 457–472 (1991)

Rigby, S.P., Edler, K.J.: The influence of mercury contact angle, surface tension, and retraction mechanism on the interpretation of mercury porosimetry data. J. Colloid Interface Sci. **250**(1), 175–190 (2002)

Rigby, S.P., Chigada, P.I., Evbuomvan, I.O., Chudek, J.A., Miri, T., Wood, J., Bakalis, S.: Experimental and modelling studies of the kinetics of mercury retraction from highly confined geometries during porosimetry in the transport and the quasi-equilibrium regimes. Chem. Eng. Sci. **63**(24), 5771–5788 (2008)

Rigby, S.P., Chigada, P.I., Wang, J., Wilkinson, S.K., Bateman, H., Al-Duric, B., Wood, J., Bakalis, S., Miric, T.: Improving the interpretation of mercury porosimetry data using computerised X-ray tomography and mean-field DFT. Chem. Eng. Sci. **66**(11), 2328–2339 (2011)

Rouquerol, J., Baron, G.V., Denoyel, R., Giesche, H., Groen, J., Klobes, P., Levitz, P., Neimark, A.V., Rigby, S., Skudas, R., Sing, K., Thommes, M., Unger, K.: The characterization of macroporous solids: an overview of the methodology. Microporous Mesoporous Mater. **154**, 2–6 (2012)

Ruthven, D.M., Xu, Z.: Diffusion of oxygen and nitrogen in 5A zeolite crystals and commercial 5A pellets. Chem. Eng. Sci. **48**(18), 3307–3312 (1993)

Salmas, C., Androutsopoulos, G.: Mercury Porosimetry: contact angle hysteresis of materials with controlled pore structure. J. Colloid Interface Sci. **239**(1), 178–189 (2001)

Satterfield, C.N., Sherwood, T.K.: The role of diffusion in catalysis. Addison-Wesley, Massachusetts (1963)

Schulz, V.P., Becker, J., Wiegmann, A., Mukherjee, P.P., Wang, C.Y.: Modeling of two-phase behavior in the gas diffusion medium of PEFCs via full morphology approach. J. Electrochem. Soc. **154**(4), B419–B426 (2007)

Tassopoulos, M., Rosner, D.E.: Simulation of vapor diffusion in anisotropic particulate deposits. Chem. Eng. Sci. **47**, 421–443 (1992)

Thommes, G., Becker, J., Junk, M., Vaikuntam, A.K., Kehrwald, D., Klar, A., Steiner, K., Wiegmann, A.: A lattice Boltzmann method for immiscible multiphase flow simulations using the level set method. J. Comput. Phys. **228**(4), 1139–1156 (2009)

Thommes, M., Skudas, R., Unger, K.K., Lubda, D.: Textural characterization of native and n-alky-bonded silica monoliths by mercury intrusion/extrusion, inverse size exclusion chromatography and nitrogen adsorption. J. Chromatogr. A **1191**, 57–66 (2008)

Tomadakis, M.M., Sotirchos, S.V.: Ordinary and transition regime diffusion in random fiber structures. AIChE J. **39**(3), 397–411 (1993)

Torquato, S., Kim, I.C.: Efficient simulation technique to compute effective properties of heterogeneous media. Appl. Phys. Lett. **55**, 1847–1849 (1989)

Torquato, S.: Random heterogeneous materials: microstructure and macroscopic properties. Springer, New York (2002)

Tsakiroglou, C.D., Payatakes, A.C.: A new simulator of mercury porosimetry for the characterization of porous materials. J. Colloid Interface Sci. **137**(2), 315–339 (1990)

Tsakiroglou, C.D., Payatakes, A.C.: Effects of pore-size correlations on mercury porosimetry curves. J. Colloid Interface Sci. **146**(2), 479–494 (1991)

Tsakiroglou, C.D., Payatakes, A.C.: Mercury intrusion and retraction in model porous media. Adv. Colloid Interface Sci. **75**(3), 215–253 (1998)

Underwood, E.E.: Quantitative stereology. Addison-Wesley, Reading (1970)

Vignoles, G.L.: Modelling binary, Knudsen and transition regime diffusion inside complex porous media. J. Phys. IV **C5**, 159–166 (1995)

Vogel, H.J., Tolke, J., Schulz, V.P., Krafczyk, M., Roth, K.: Comparison of a Lattice-Boltzmann model, a full-morphology model, and a pore network model for determining capillary pressure-saturation relationships. Vadose Zone J. **4**(2), 380–388 (2005)

Wilke, C.R., Lee, C.Y.: Estimation of diffusion coefficients for gases and vapors. Ind. Eng. Chem. **47**(6), 1253–1257 (1955)

Zalc, J.M., Reyes, S.C., Iglesia, E.: The effects of diffusion mechanism and void structure on transport rates and tortuosity factors in complex porous structures. Chem. Eng. Sci. **59**(14), 2947–2960 (2004)